Department of AERONAUTICS and ASTRONAUTICS
STANFORD UNIVERSITY

(NASA-CR-162441) THERMAL-PROTECTION MATERIAL EVALUATION AND DIAGNOSTIC STUDY OF ADVANCED HIGH-POWER ARC JETS FOR PLANETARY ENTRY SIMULATION Final Technical Report, 1 Jul. 1976 - 30 Jun. 1979 (Stanford Univ.)
N80-70349
Unclas
00/24 46075

Final Technical Report

July 1, 1976 - June 30, 1979

THERMAL-PROTECTION MATERIAL EVALUATION AND DIAGNOSTIC STUDY OF ADVANCED HIGH-POWER ARC JETS FOR PLANETARY ENTRY SIMULATION

NASA Grant No. NSG-2166

Submitted to the

National Aeronautics and Space Administration

Ames Research Center

Moffett Field, California 94035

Philip Nachtsheim - Technical Officer

by the

Department of Aeronautics and Astronautics

Stanford University

Stanford, California 94305

Donald Baganoff - Principal Investigator

George Liu - Research Associate

October 1979

Final Technical Report

July 1, 1976 - June 30, 1979

THERMAL-PROTECTION MATERIAL EVALUATION AND DIAGNOSTIC STUDY OF ADVANCED HIGH-POWER ARC JETS FOR PLANETARY ENTRY SIMULATION

NASA Grant No. NSG-2166

Submitted to the

National Aeronautics and Space Administration

Ames Research Center

Moffett Field, California 94035

Philip Nachtsheim - Technical Officer

by the

Department of Aeronautics and Astronautics

Stanford University

Stanford, California 94305

Donald Baganoff - Principal Investigator

George Liu - Research Associate

October 1979

INTRODUCTION

This is a Final Technical Report for NASA Grant No. NSG-2166 covering the period July 1, 1976 to June 30, 1979. The primary objective of this grant was to conduct an experimental research program for the evaluation of various heat-shield materials for use in planetary entries. The program has immediate applications to the upcoming NASA Jupiter Orbitor-Probe mission or Project Galileo and as a matter of fact the bulk of the research work was conducted in support of this mission. A significant portion of the experimental effort encompassed the initial calibration, instrumentation, and design support of the NASA-Ames Research Center's 100 MW, high-enthalpy, constricted-arc plasma jet, or the Giant Planet Facility (GPF). Techniques and experience gained in these areas are considered valuable for application to the 160 MW High Enthalpy Entry Facility currently under construction at Ames.

The report gives a summary of the experimental facility, its instrumentation and diagnostics, and test results to date. For chronological progress and development of this study, the reader is referred to the Semi-Annual Progress Reports covering the period July 1976-December 1978.

EXPERIMENTAL FACILITY

The Giant Planet Facility is an Ames-developed, electric-arc, plasma-jet facility capable of simulating the heating environments for entries into the atmospheres of the outer planets. It is rated at 100 MW and operates with a hydrogen-helium gas mixture to produce a stagnation-flow region with simultaneous high radiative and convective heating.

These features make it particularly suitable, and hitherto unavailable, for simulation of the heating environment for a Jovian planetary probe.

The stagnation-point heat-transfer rates for the entry probe of the Galilean mission have been computed for nominal entry conditions[1] and are shown in Figure 1. It should be recognized that the calculated rates can change as the atmospheric model changes and as refinements are introduced into the complex heat-transfer theories. The overall heating magnitude and its relative radiative and convective components, however, will remain correct. The heating at the nose is dominated by the radiative component, which has a peak value of 59 kW/cm^2 and occurs over a pulse length of 12 sec. The convective heating has a peak value of 18 kW/cm^2 and a pulse length of 21 sec. Impact pressure increases only slightly during the heating pulse and is between 5 and 6 atm at peak conditions.

These heating rates are so high that the heat shield, even with high-performance graphitic materials together with the so-called optimum heat-shield design, will constitute a major portion of the entry mass.[2] Consequently, the performance of the heat shield assumes a critical role in determining the success of the mission. However, major shortcomings exist in the technology for heat-shield design for this application: (1) no experimental data exist regarding the absorption effects of the ablation vapors in coupled convective and radiative heating environments with massive boundary-layer blowing; and (2) the analytical models of the ablative performance of carbonaceous materials under conditions of very high radiation are uncertain.[3] This lack of information, coupled with the uncertainty in material response in the coupled heating

environment established the need for an experimental facility to simulate the Jupiter heating case.

The GPF is shown schematically in Figure 2. It consists of a 6-cm diameter constricted-arc heater coupled directly to a low-Mach-number, supersonic nozzle (M = 1.67). The nozzle discharges as a free jet into a walk-in test chamber that is 2.6 m on a side. The test models are mounted on four quick-acting sting supports. Precise sting insertion time and exposure duration are controlled by a programmable timer that is an ancillary part of an automatic gas-flow control system. The test chamber exhausts into a 5-stage steam ejector system during the starting mode and is vented into atmosphere during the high-pressure running mode. Direct current for the arc heater is provided by a power supply consisting of six modules, where each consists of a three-phase, full-wave, phase-controlled rectifier. Cooling water for the arc heater is supplied by 10 high-pressure water pumps with a total flow rate of 500 kg/sec.

The use of hydrogen as a component of the test gas requires special precautions to ensure safe system operation. Because the facility uses an electric arc for heating, an ignition source is always present; therefore, the facility is operated such that air is not permitted to come into contact with the working gas in the arc heater, test chamber, or the exhaust system. The arc heater is enclosed within a large duct and a fan, rated at 12,000 ℓ/sec, draws air over the facility and exhausts it outside the building. This air flow, when mixed with the maximum hydrogen leak possible for the facility, results in a mixture considerably below the detonation limit (18% by volume).

In the test chamber, nitrogen is added to the hydrogen-helium test gas during the run to dilute it to the point where the mixture will not burn when it is exhausted into the atmosphere. After each run, nitrogen is used to purge the system of hydrogen. When the test conditions are such that the nozzle exit pressure is below 1 atm, the test gas is discharged into the vacuum system. The hydrogen-helium test gas, in this case, is further diluted by steam or water vapor while it is in the condenser of the steam ejector system, thus providing an additional margin of safety.

The 6-cm diameter constricted-arc heater is the principal component of the GPF. This arc heater is a result of a design philosophy that evolved at Ames Research Center over a number of years.[4,5] The basic principle underlying this type of arc heater is the operation at very high levels of current density which raises the resulting arc temperature to very high levels. This is accomplished by constricting the arc discharge which causes the voltage gradient to increase along with the temperature. In order to avoid an arc attachment to the confining wall under such high voltage-gradient operation, the constrictor tube must be formed of thin discs such that the arc-column voltage drop along each disc is considerably less than the voltage breakdown level for the discs. This accounts for the characteristic stacked-disc construction of the constricted-arc heater. For the GPF arc heater, the constrictor tube is in modular form with each module containing 24 electrically isolated constrictor discs of 1 cm thickness and 6 cm inside diameter. A clear plastic material is used as the potting agent for the modules; it permits visual inspection of the discs for signs of inadequate cooling. Eighteen

modules, mounted end-to-end, form the constrictor tube of 4.32 m in total length.

To accommodate the high current with low contamination levels, the anode assembly is designed with 10 parallel-connected, water-cooled copper rings as electrodes. Each electrode is capable of operation up to 1000 A and the arc termination point is driven around the interior surface by a magnetic field generated by a coil located within the electrode. The cathode arrangement is considerably different from that of any other system. For very high enthalpy levels, the arc should terminate in the supersonic nozzle as close to the test section as possible. To reduce radiative and convective losses, this consideration ruled out a conventional cathode location in a plenum ahead of the nozzle. Four graphite cathodes are arranged in a symmetrical pattern 10 cm from the nozzle exit. The cathode tips are beveled and are located 15 cm from the centerline of the nozzle so that, at full pressure operation, they are well outside the test stream and avoid any interference effects. Although the graphite electrodes show wear, spectroscopic measurements at the stagnation point of test bodies revealed carbon-particle contamination of the test stream to be minimal. To date, this anode-cathode configuration has operated reliably up to power levels of 80 MW.

Since radiation is the dominant heating mechanism for the Jupiter probe heat shield, it is important to attain maximum values of stagnation temperature, pressure, and shock stand off distance in the test facility. This requires an optimization of the nozzle and test body design. Previous studies showed that in order to obtain high radiation

heating in arc-jet flow, a blunt body shape is necessary to provide a large radiating volume within the gas cap.[6] Parametric analyses were made for such a body to obtain an optimum nozzle configuration.[1] The analysis shows that the radiative heating to a test body decreases as the Mach number of the facility increases. The decrease in the heat-transfer rate is caused by the reduction in stagnation pressure associated with the normal shock pressure recovery that occurs with increasing Mach number. Maximum radiative heating is predicted for a Mach number of 1.60. The analysis shows that the convective heat-transfer rate also decreases as the Mach number increases. From these considerations of the heating capabilities of the arc-jet system, the Mach number selected for the GPF was 1.67, which represents a slight compromise of the heat-transfer rate to allow for an increase in the physical size of the test body.

The nozzle was specified to be a simple conical shape with a half-angle of 0.94° and an exit diameter of 7 cm. The expansion is so slight that contouring of the walls is not warranted to obtain an essentially uniform, parallel nozzle exit flow. The pressure ratio between the total (or arc heater) pressure and the nozzle exit pressure for an ideal free jet is 4.41 from isentropic nozzle flow relations ($\gamma = 1.23$). Accordingly, the arc pressure must be 4.41 atm for an atmospheric-vented test chamber which happens to be slightly less than the 5-atm-rated operating pressure of the arc jet.

INSTRUMENTATION AND DATA ACQUISITION SYSTEM

The test stream instrumentation program of the GPF was tailored to measure the heat-transfer rate to the model surface, its surface temperature, pressure, and ablation rate. Principal methods and tools include

thin-slug calorimeter, bolometer, pressure probe, pyrometer, laser shadowgraph and rapid-scan optical spectrometer. The pyrometer and rapid-scan optical spectrometer were all commercial units and no attempts will be made to describe them other than to say they performed adequately. The rest of the diagnostic instruments were designed and made specifically for the GPF and a brief description of them will be given.

Due to the intense heat-transfer rates encountered at the GPF, steady-state, water-cooled calorimeters cannot be used to make the heating measurements. The transient asymptotic calorimeter, such as the null-point type, which is rapidly swept through the test stream was not adaptable because the elctromagnetic noise associated with the high-power arc resulted in an unacceptable signal-to-noise ratio. Consequently, the thin-skin, transient calorimeter design shown in Figure 3 was adopted to measure the total cold-wall, heat-transfer rate to the test model. 40-mil thick tungsten, formed by sintered metallurgy process, was chosen as the slug material after a heating analysis recognizing the requirements of fast response time (< 5 mS) and relatively long service life (~ 50 mS). The spring-loaded thermocouple employed ensured good thermal contact with the cap during any motion caused by thermal stresses, but the contact resistance associated with spring loading introduces the need for individually calibrating the calorimeter.

The calibration was performed using a black-body radiation source and a xenon lamp with a heat flux of up to 2 kW/cm^2. When the calorimeter was used in the GPF, a Telfon sabot was placed over the tungsten cap to protect it during the time required to insert the calorimeter

into the stream centerline; this approach minimized any pre-heating of the tungsten before reaching the centerline and hence maximized its useful life span.

While the calorimeter measures the combined convective and radiative heat fluxes, the bolometer measures the radiation intensity only. The design was one evolved directly from an earlier study[6] and is shown schematically in Figure 4. It consists of two thermally isolated and blackened radiation sensors embedded in a body with the same geometry as the test model. Each sensor is well collimated to view only a very small solid angle (~ 10^{-4} ster) of the test stream and is shielded from the convective heating by a gas-purged magnesium fluoride window. The two-sensor approach gives a measurement of the radiation distribution around the test model and with such a distribution, a total radiation flux can be estimated.

Two designs had been used for the pressure probe which has the same geometry as the test model except for pressure taps at various locations. Originally, piezoelectric detectors were embedded in an all-metal body, which worked fine other than being totally destroyed after each run. This was modified to a graphite body design with ducts connected to detectors outside of the test chamber. Without destroying the piezoelectric detectors at each run, and thereby saving tremendous expenses, the graphite design proved to be adequate both in time response and durability in the data acquisition period. They were used extensively in measuring the pressure profile at the test model, which also indicates the test-stream Mach number, under different arc running conditions.

Due to the intense radiation of the gas cap in front of the test

model, conventional photography or cinemagraphy tends to give poor results for the recording of the model ablation rate simply because the shock layer radiation overshadows and masks all interior details. Instead, a laser shadowgraph system, shown in Figure 5, was designed for flow visualization. Its principal component is a 5-watt, continuous wave argon ion laser with the beam expanded to cover a 5-inch diameter area of the test section; the relatively high intensity of the laser will dominate the gas cap radiation at its narrow bandpass centered at 5145 A. The whole system was mounted on optical benches supported by air bearings to isolate it from vibrations; it was also entirely encapsulated and interlocked for safety purposes.

The data acquisition system utilized two separate but compatible modes of operation. Arc operating parameters such as voltage, current, mass flow rate, pressure, constrictor wall heating rate, etc., were fed into a digital scanner and integrating voltmeter (Vidar) which was operated normally at one complete cycle per second. The data were stored in an on-line computer (Wang) which also reduced, printed and plotted the arc parameters after each run. This is a proven system but the drawback is mainly storage capacity and relatively slow processing speed. An effort was initiated to switch these operations to a more versatile and powerful system (Teledyne).

The test data such as calorimeter, pressure probe and pyrometer outputs which required complete documentation for each run were recorded by a multi-channel, high speed, fiber-optic cathode-ray tube oscillograph (Honeywell Visicorder). The analog data, in most cases, were reduced manually which proved to be somewhat cumbersome. Depending on

the kind of information that was required, the raw data could be processed through a bank of amplifiers and band-pass filters before being recorded.

To ensure safety in view of the dangerous high voltage and current present during arc operation, all arc-parameters, diagnostic, and data transducers were all powered and enclosed in an electrically isolated environment from the recording and control system, with optical fibers being the data transmission lines. These safety precautions proved to be invaluable during several incidents when an external arc was found to have struck.

CALIBRATION AND TEST RESULTS

Since maximizing the heat transfer rate to the test model is one of the most important tasks in the GPF calibration program, the heat transfer rate as measured by the thin-slug calorimeter was viewed as the critical parameter in evaluating various arc running conditions. For a given arc running condition, two main modes of operation were investigated - one with the arc exit, or test chamber, pressure maintained by a vacuum system and the other with the arc exhausted essentially into the atmosphere. At a nominal power level of 60 MW, results indicated that with the exit pressure maintained at 0.2 atm, the measured total heat transfer rate was approximately 15 kW/cm^2 at a test Mach number of 3.0. When the arc was vented into the atmosphere, the measured total heat transfer rate was increased to 20 kW/cm^2 accompanied by a jump in stagnation pressure. This finding agreed with Mach number effect since venting to atmospheric pressure resulted in a test Mach number, dictated primarily by arc and test chamber pressure ratio, closer to

the designed nozzle Mach number of 1.7, which theoretically maximizes the heat transfer rate. Ideally, for every arc pressure level, one should set the test chamber pressure so that a matched expansion exists at the nozzle exit. However, due to the lack of control of test chamber pressure, all high power (and pressure) runs were operated with the exhaust venting into the atmosphere.

Figure 6 shows the measured heat transfer rate as a function of power input. All the results were obtained by using an equal mixture of hydrogen and helium. The solid lines represent predictions obtained by semi-empirical scaling laws outlined in Reference 1. Though the heat transfer rate increased tremendously as the arc power was raised, arc failure became an increasing occurrence above a threshold of 60 MW. A decision was made that rather than risk the possibility of a massive failure by increasing the power of the GPF, a test program of the candidate heat-shield materials for the Jupiter probe should be carried out as soon as the maximization of the heat transfer rate was accomplished at the power level of 60 MW.

Table 1 shows a typical set of arc operating conditions at which the material test program was carried out. The values shown represent averages of a large number of runs. For an actual test run, the parameters obtained for that particular run were used for data reduction. Table 2 shows a comparison between the flight environments experienced by a carbon phenolic heat shield at peak heating during Jovian entry and the simulation provided by the GPF. Though the flight stagnation point heating rate far exceeds that provided by the arc jet, namely, 12.3 kW/cm^2 convective and 6.0 kW/cm^2 radiative, the GPF does simulate

to a great extent the environment encountered at the flank region - an area that accounts for 80-90% of the heat shield weight. In addition, the simulation approximates the flight environment of the entire heat shield for a significant time portion during entry.

The spectrum of test materials encompasses graphites, composites and silica, supplied mostly by the heat shield contractors. Typically, models of a given material were inserted into the test stream for various periods up to about 7 sec. Mass loss and surface recession were obtained by before- and after-run measurements and a plot versus time-in-stream yields the steady-state mass-loss and recession rates. Results for chop-molded carbon phenolic, which are typical of the data obtained, are shown in Figure 7. The surface recession rate can also be delineated by the laser shadowgraph movie - a more laborious process - and, in general, the results from the two approaches agreed.

Table 3 shows a summary of the data. The consistency of the GPF performance was demonstrated by the two different sets of ATJS 4 cm data, obtained throughout the test span, showing identical ablation results. The graphitic materials - ATJS, ATJ, 3-D carbon - are comparable as a group and performed best under the applied heating rate of 18.3 kW/cm^2. The mass-loss rates of different carbon phenolics varied significantly, ranging from a low for GE 20° laminate - comparable to that of graphite - to a high for MDAC 35° laminate. The apparent discrepancy between the surface recession and mass loss for MDAC inverse chevron was explained by the high vaporization rate of its binder material. MDAC silica was the poorest of the ones tested but this was expected since its heat accommodating mechanism was optimal

for a high radiative environment, which was not the test case. It would be erroneous to simply conclude that graphitic materials should be chosen as heat-shield materials for the Jovian entry environments. This is due to the fact that their thermal conductivity is extremely high, thereby requiring an insulating layer, which could lead to a higher thermal protection system weight than, say, one of carbon phenolics.

Material spallation, a serious concern that could lead to massive failure of the heat shield, was not observed for all samples tested on the basis of either the laser shadowgraph/movie system or post-run model examination. The applied heat flux, however, was only about half of that predicted by several generally still unsubstantiated, theories for such a phenomenon. This will be a particular area of interest as the GPF is increased in power to achieve higher heating rates.

A feasibility study program was also carried out to utilize the unique GPF features for the testing of the Jupiter probe aft-body heat shield. The basic requirements were a large test body subjected to an applied heating rate of 1 kW/cm^2 in a hydrogen/helium atmosphere. After experimenting with several arc running and test configurations, the requirements were met for a scaled model of up to 25.4 cm in diameter. The arc was run at 12.4 MW with the nozzle exit, or test chamber, pressure maintained at 0.07 atm. The highly expanded free jet gave rise to a fairly uniform heating rate to the model placed at 79 cm downstream of the nozzle.

REFERENCES

1. Winovich, W. and Carlson, W.C.A., "The Giant Planet Facility," presented at the 25th International Instrumentation Symposium, Anaheim, California, May 1979.

2. Nicolet, W.E., Howe, J.T. and Mezines, S.A., "Outer Planet Probe Entry Thermal Protection: Part II: Heat-Shielding Requirements," AIAA Paper no. 740701, AIAA/ASME Thermoplysics and Heat Transfer Conference, Boston, Massachusetts, July 1974.

3. Nelson, H.F. and Mezines, S.A., "Parametric Analysis of Jupiter Probe Heat Shield Recession Uncertainties," AIAA Paper no. 78-919, Second AIAA/ASME Thermophysics and Heat Transfer Conference, Palo Alto, California, May 1978.

4. Stine, H.A. and Watson, V.R., "The Theoretical Enthalpy Distribution of Air in Steady Flow Along the Axis of a Direct-Current Electric Arc," NASA TN D-1331, 1962.

5. Shephard, C.E. et al., "A High Enthalpy Plasma Generator for Entry Heating Simulation," NASA TN D-4588, 1968.

6. Winovich, W., "Total Radiation at the Stagnation Point of Blunt Bodies at Stagnation Temperatures to 15000 K." AIAA Paper no. 68-405, AIAA 3rd Aerodynamic Testing Conference, San Francisco, California, April 1968.

FIG. 1 STAGNATION-POINT HEAT TRANSFER AND PRESSURE FOR THE ENTRY PROBE

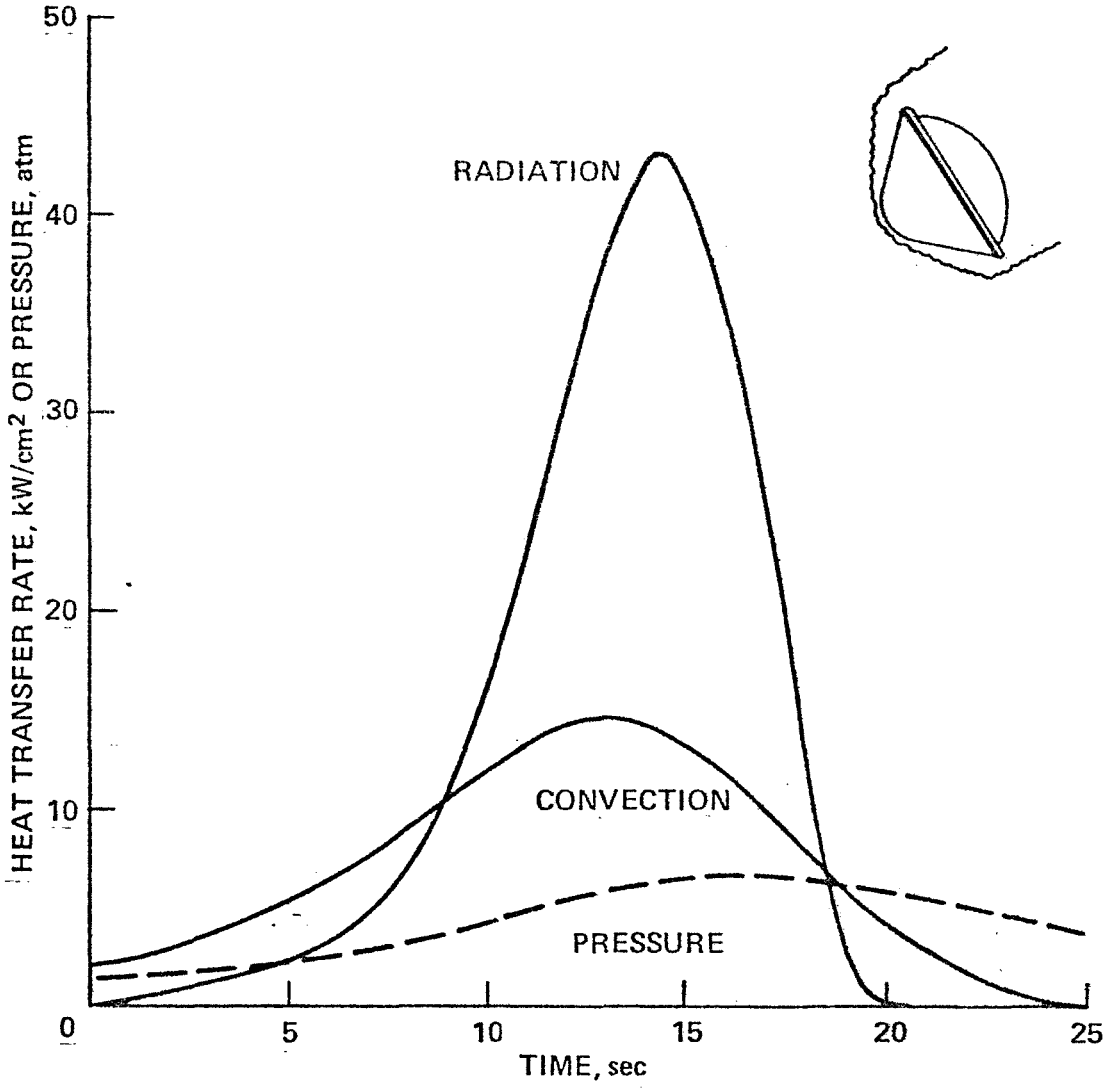

FIG. 2 THE GIANT PLANET FACILITY

GPF SPECIFICATIONS

CONSTRICTOR DIAMETER ..... 6 cm
CONSTRICTOR LENGTH ..... 432 cm
RATED CURRENT ..... 8000 A
RATED PRESSURE ..... 5 atm
RATED POWER ..... 100 MW
ENTHALPY .. .. 400 - 500 MJ/kg

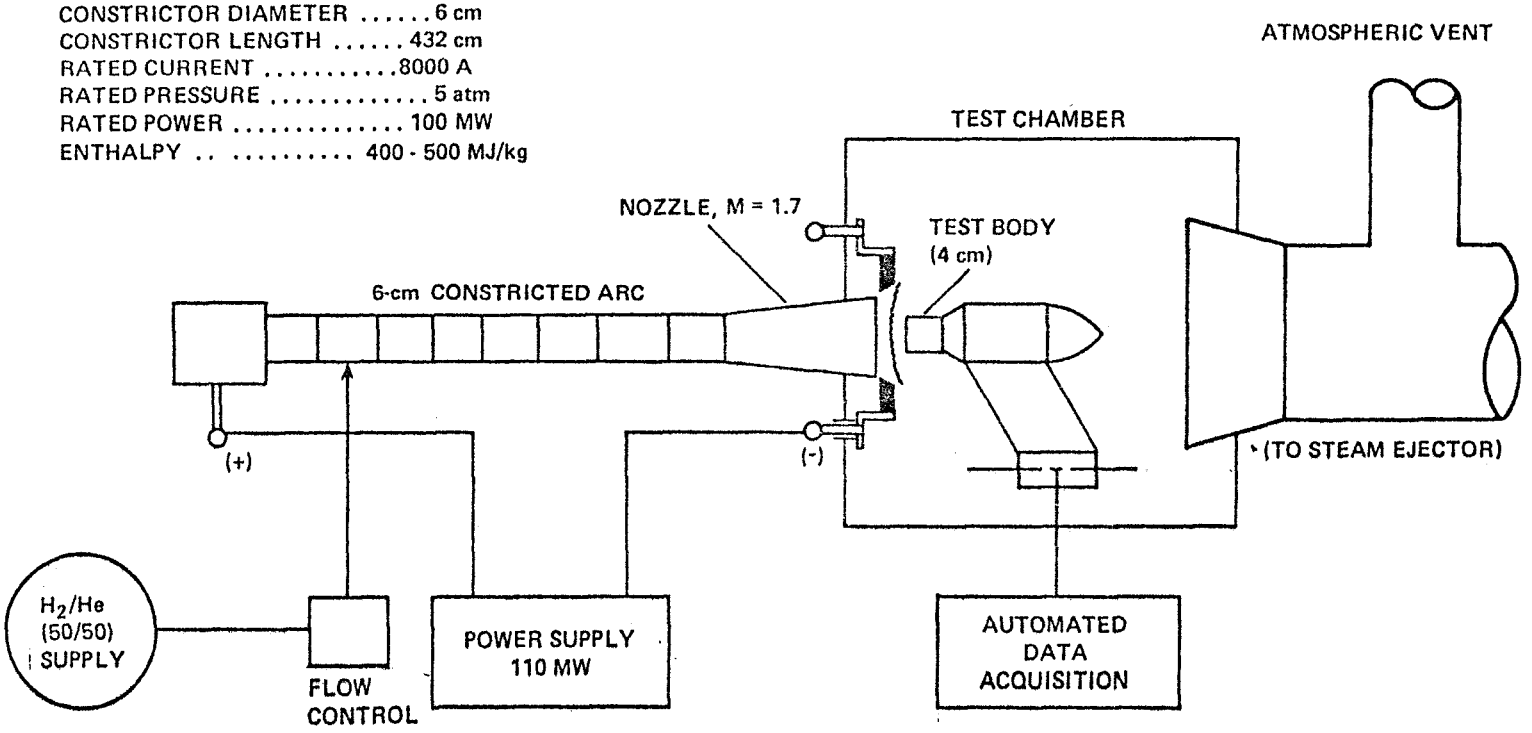

FIG. 3 CALORIMETER DEVELOPED FOR HIGH HEATING RATES

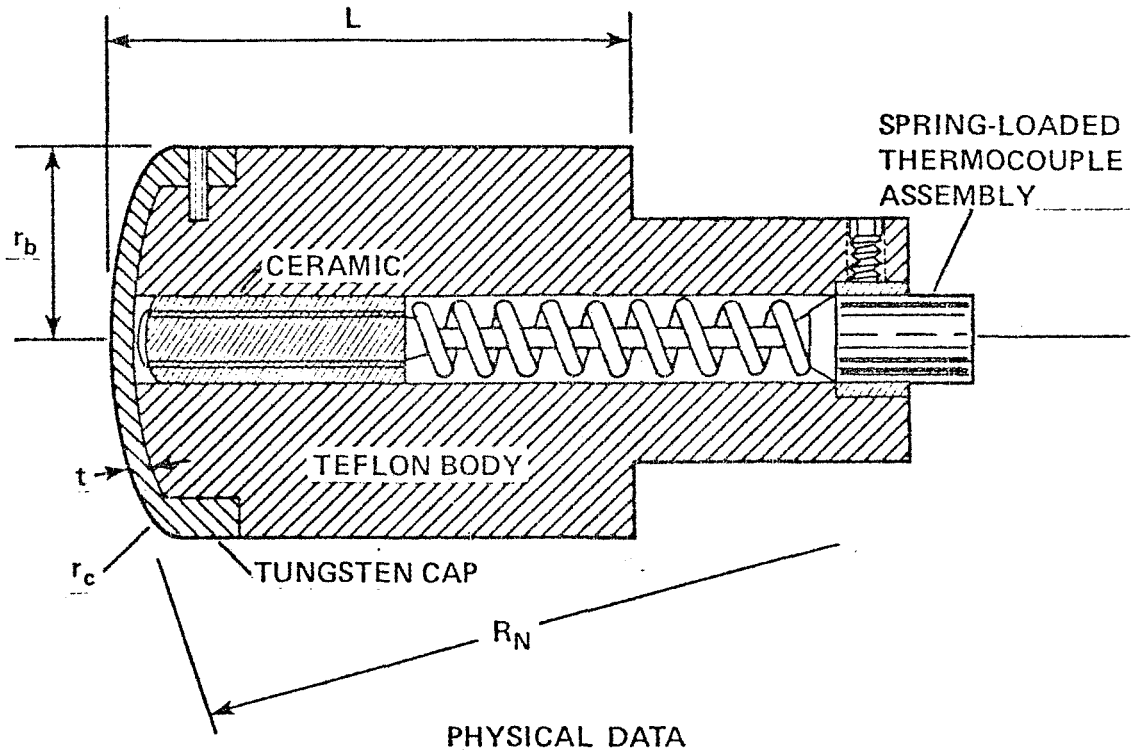

PHYSICAL DATA

r_b = 2.06 cm
r_c/r_b = 0.20
R_N/r_b = 10.00
L/r_b = 5.62
THERMOCOUPLE:
CHROMEL-ALUMEL
SENS. = 0.04 mV/°C
SURFACE: 0.20 μ,
rms, GROUND
t, THICKNESS = 1.02 mm

FIG. 4 RADIATIVE INTENSITY PROBE
(BOLOMETER)

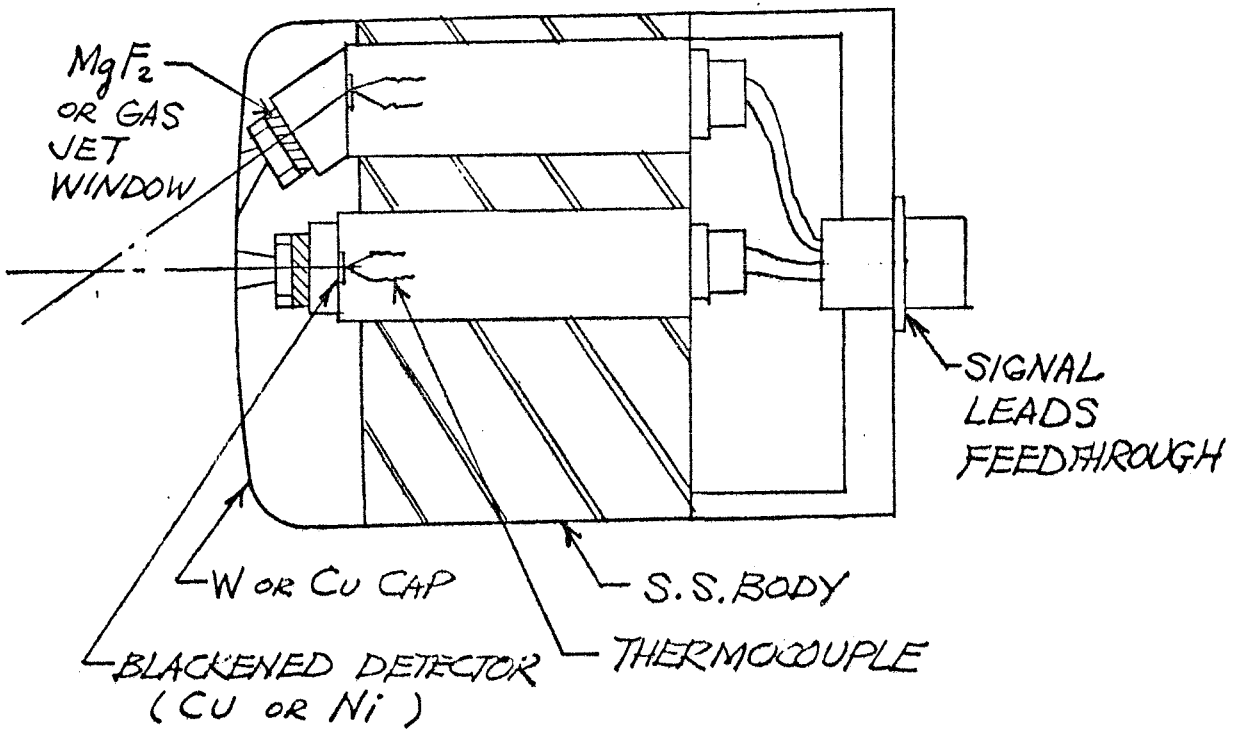

FIG. 5 LASER SHADOWGRAPH SYSTEM

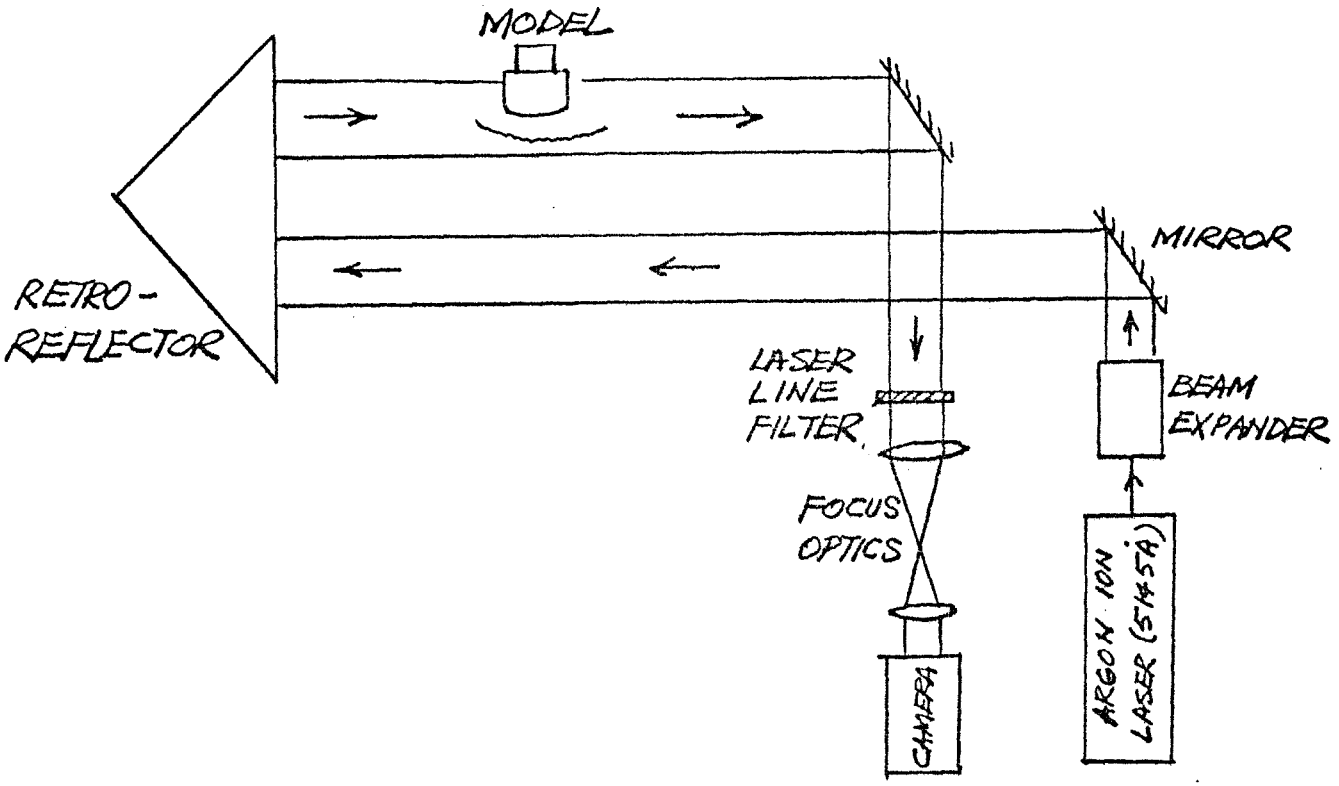

FIG.6 HEAT TRANSFER RATES IN THE GIANT PLANET FACILITY

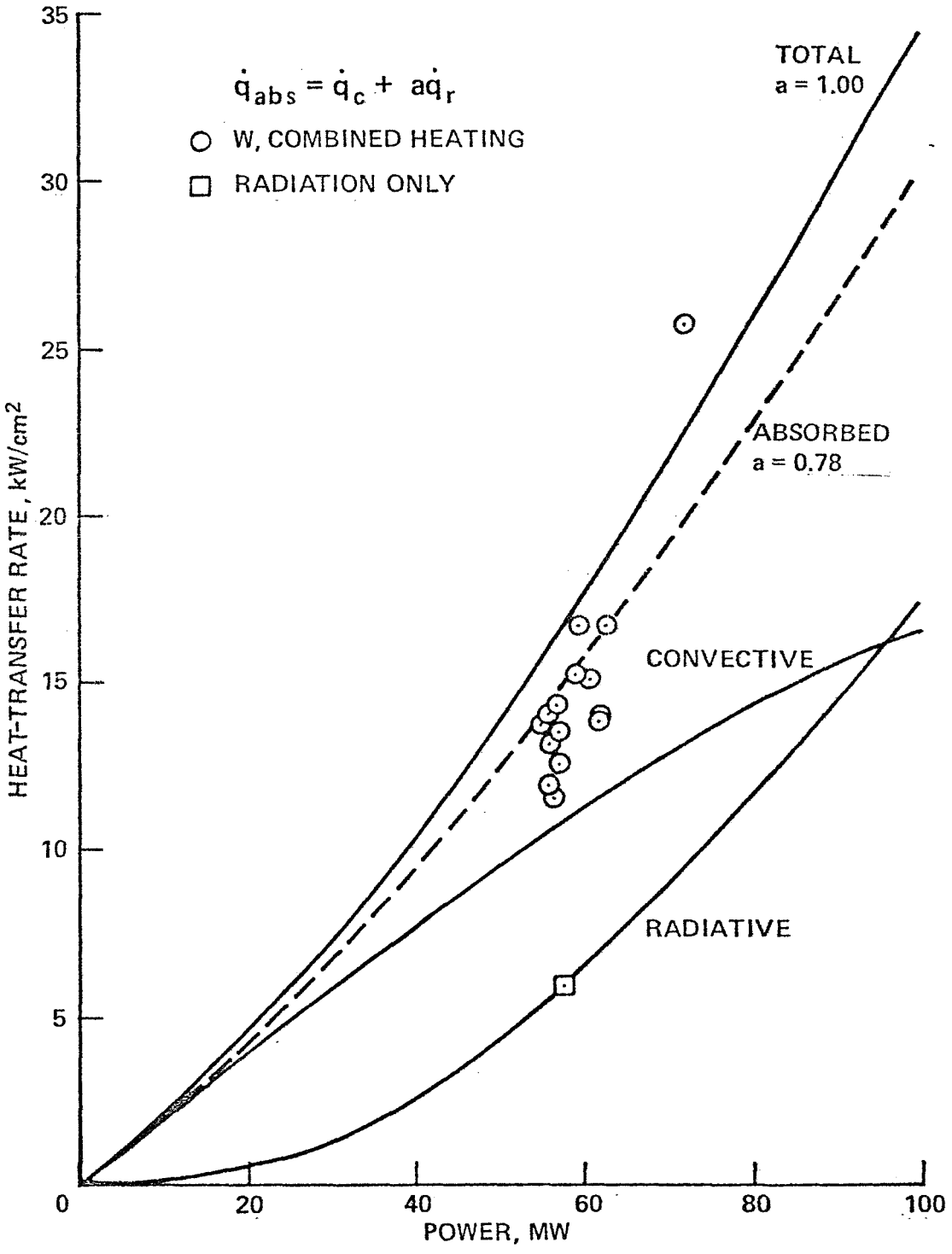

FIG. 7 ABLATION RESULTS

CHOP MOLDED CARBON PHENOLIC

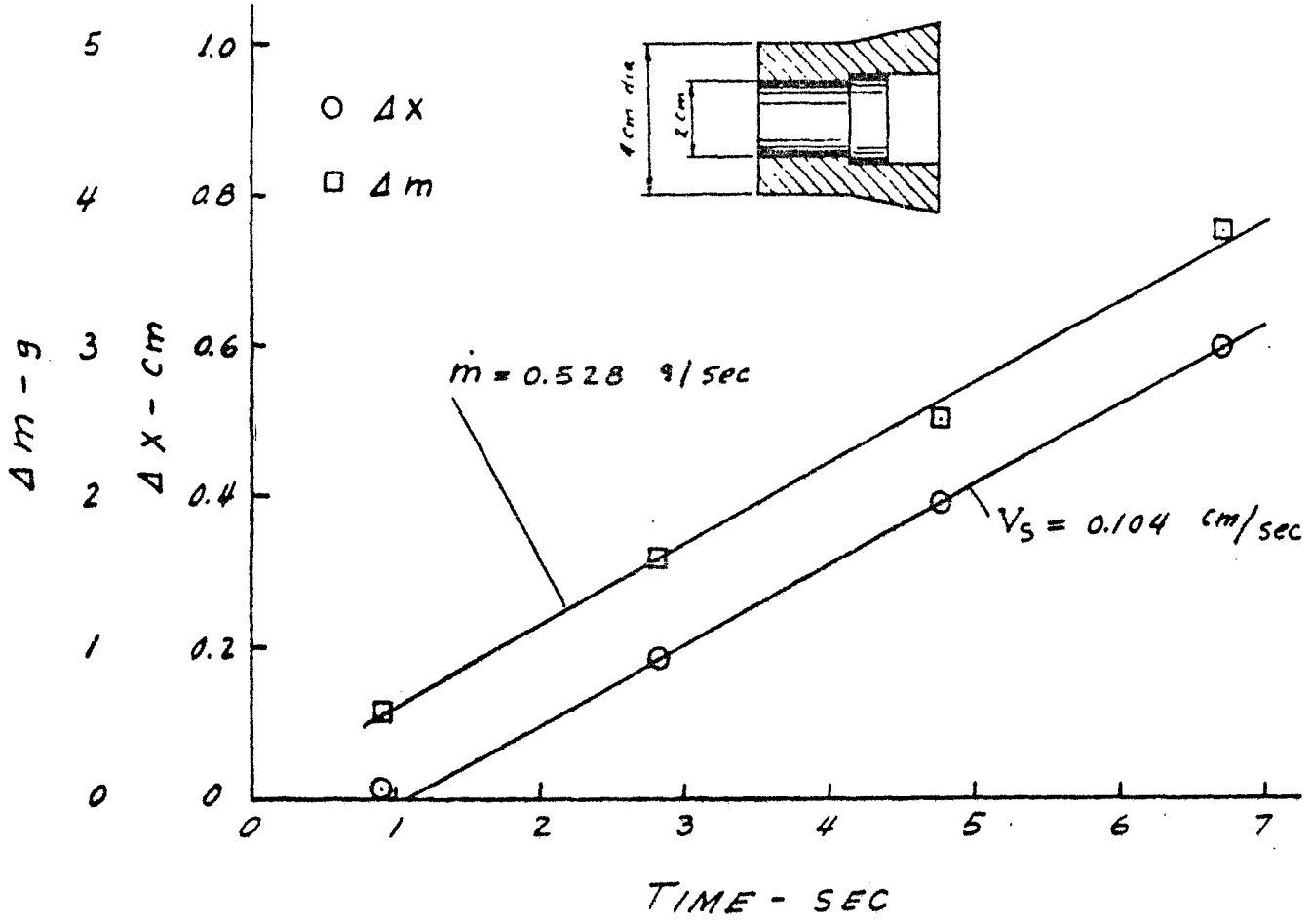

TABLE 1. TEST CONDITIONS IN ARC JET

Gas Composition	H_2/He - 50/50 by vol
Arc Power	57.7 MW
Current	5.33 kA
Voltage	10.8 kV
Flow Rate	0.123 kg/sec
Bulk Enthalpy	185 MJ/kg
Centerline Enthalpy	370
Arc Pressure	3.8 atm
Model Stagnation Pressure	2.2
Test Chamber Pressure	1.0
Mach Number	1.4 ~ 2.1
Measured Convective Rate	12.3 kW/cm^2
Measured Radiative Rate	6.0
Model Size	4 cm dia flat face

TABLE 2. SIMULATION REQUIREMENTS

Carbon Phenolic Heat Shield

	FLIGHT		ARCJET
	Peak Heating		4 cm Model
	STAG PT	FLANK	
Gas Composition, H_2/He by vol	89/11		50/50
Applied Radiative Rate, kw/cm^2	40.3	8.2	6
Applied Convective Rate	14.9	8.9	12.3
Net Radiative Rate	20.2	11.7	5 - 6
Net Convective Rate	0	1.2	
Surface Pressure, atm	5.4	2.9	2.2
Enthalpy, MJ/kg	860		370
Shock Layer Temperature, K	16,100	12,300	14,000 $\pm$ 1000
Shock Standoff Distance, cm	3.0	8.5	2.5

TABLE 3. DATA SUMMARY

TESTS IN GIANT PLANET PILOT FACILITY

Material	Model Dia, cm	Model Shape	V_s cm/sec	Density g/cm^3	Mass-Loss Rate g/cm^2 sec
ATJS Graphite	4	FLAT	0.070	1.83	0.128
ATJS Graphite	4	FLAT	0.070	1.83	0.128
ATJS Graphite	2	FLAT	0.097	1.83	0.177
ATJS Graphite	1	FLAT	0.140	1.83	0.256
ATJS Graphite	4	HEMI	0.105	1.83	0.192
ATJ Graphite	4	FLAT	0.067	1.73	0.116
FMI 3-D Carbon-Carbon	4	FLAT	0.078	1.74	0.136
GE 20^{o} Laminate Carbon Phenolic	4	FLAT	0.087	1.45	0.127
GE Chop Molded Carbon Phenolic	4	FLAT	0.104	1.45	0.168
MDAC 35^{o} Laminate Carbon Phenolic	4	FLAT	0.108	1.45	0.221
MDAC Inverse Chevron Carbon Phenolic	4	FLAT	0.081	1.45	0.213
MDAC Silica	4	FLAT	0.150	1.95	0.292